Advanced Steel Construction – Vol. 22 No. 3 (2026) 286–297
DOI:10.18057/IJASC.2026.22.3.4

STUDY ON POST-FIRE MECHANICAL PERFORMANCE OF Q460QENH WEATHERING STEEL WITH THREE COOLING METHODS

Bing-Sen Wang [1], Hang Yin [1, 2, *], Li-Juan Zheng [3], Er-Nian Zhao [1] and Kai Yan [1]

[1] *Key Laboratory of Building Structural Retrofitting and Underground Space Engineering (Shandong Jianzhu University), Ministry of Education, Jinan 250101, China*
[2] *Collage of Civil Engineering, Tongji University, Shanghai 200092, China*
[3] *Shandong Lukan Group Co., Ltd, Jinan 250101, China*
** (Corresponding author: E-mail: yinhang@tongji.edu.cn)*

ABSTRACT

Monotonic tensile tests were performed to investigate the mechanical behavior of Q460qENH weathering steel after exposure to temperatures ranging from 20°C to 1000°C, considering three different cooling methods: cooling in air (CIA), cooling in water (CIW), and cooling in fire-fighting foam (CIF). The tensile fracture surfaces were analyzed using scanning electron microscopy (SEM), and the post-fire mechanical properties were systematically evaluated. The results revealed that the fracture surfaces under CIA and CIF conditions exhibited similar dimple morphologies, while the number of dimples decreased progressively with increasing temperature under CIW conditions. Both the cooling method and the exposure temperature exerted only a limited effect on the elastic modulus. A distinct yield plateau in the stress - strain curve disappeared under all cooling conditions after exposure to temperatures of 800 °C or higher. Under CIA and CIF conditions, the yield strength decreased markedly after exposure to temperatures above 600 °C, while the ultimate tensile strength remained relatively stable. In contrast, under CIW conditions, the yield strength initially declined but recovered to nearly its original value after exposure to 700 °C, accompanied by a pronounced increase in ultimate strength. The CIW process was found to reduce ductility but enhance Brinell hardness. Furthermore, a mathematical model was developed to describe the post-fire mechanical properties under different cooling conditions, providing theoretical support for assessing the residual load-bearing capacity of steel structures following fire exposure.

ARTICLE HISTORY

Received: 27 March 2025
Revised: 23 August 2025
Accepted: 23 August 2025

KEYWORDS

Q460qENH weathering steel;
Cooling methods;
Monotonic tensile;
Post-fire mechanical properties;
Mathematical model

1. Introduction

Weathering steel is a high-performance structural steel commonly used in bridge construction without the need for additional protective coatings. However, weathering steel bridges may be exposed to extreme events during their service life, such as fires caused by traffic accidents, spontaneous vehicle combustion, or electrical failures [1-2]. The unpredictable nature of these incidents, combined with the difficulties associated with firefighting, can result in severe damage to critical structural components, potentially leading to the decommissioning or even demolition of entire bridges [3-5]. Existing design codes for steel structures primarily focus on fire protection in buildings. Therefore, understanding the post-fire mechanical properties of weathering steel is essential for ensuring the safety and reliability of high-performance weathering steel bridges, and has consequently become a key topic in recent research.

Studies have shown that the post-fire mechanical properties of different steels are strongly affected by factors such as manufacturing processes, steel grades, and fire exposure conditions. Song [6] investigated the influence of thermomechanical controlled processing (TMCP) and quenching - tempering (QT) treatments on the post-fire mechanical properties of high-strength structural steels. Wang [7] examined the effects of fire exposure temperature, cooling methods, heating rates, and initial loading conditions on the post-fire mechanical performance of Q690 high-strength steel. The results indicated that high heating rates, repeated heating and cooling cycles, and axial loading conditions significantly reduced both the elastic modulus and yield strength. Qiang [8] studied the post-fire performance of S960 ultra-high-strength steel, revealing substantial differences compared to S460, S690, and low-carbon steels. The study identified 600 °C as the phase transformation temperature for S960 steel and proposed an empirical model to predict its post-fire mechanical properties based on experimental data. Li [9] analyzed the effect of heating rates on the post-fire mechanical behavior of high-strength steels and concluded that the heating rate had minimal influence on their performance. Ren [10] investigated the post-fire mechanical properties of Q235 cold-formed steel sections, finding that member thickness had a negligible effect, whereas notable differences in mechanical performance were observed between flat and curved regions.

The influence of fire extinguishing methods on the material properties of steel structures is also of considerable importance. Notable variations in post-fire mechanical properties have been observed among different steel grades [11-13]. Zhang [11] investigated the effects of foam and water immersion cooling on the post-fire mechanical behavior of Q355 steel, reporting that when the exposure temperature exceeded 600 °C, the yield strength and ultimate tensile strength of specimens decreased under CIF conditions, whereas those under CIW conditions increased significantly. Zhou [12] examined the mechanical properties of Q620 high-strength steel under CIA, CIW, and CIF conditions, observing minimal differences between CIA and CIF, but substantial disparities between CIW and the other two cooling methods. Zhang [13] studied the post-fire mechanical behavior of Q345 structural steel subjected to repeated heating and cooling cycles between 200 °C and 900 °C under CIF conditions. With an increasing number of thermal cycles, pronounced degradation was observed in yield strength, ultimate tensile strength, and fracture elongation.

Q460qENH steel is a widely used high-strength steel developed in recent years for bridge construction in China. It has a minimum yield strength of 460 MPa. The letter “E” represents the quality grade, indicating that the steel satisfies the requirements of the -40 °C impact test, thereby ensuring good toughness even in low-temperature environments. The letters “NH” signifies the steel’s excellent resistance to atmospheric corrosion. However, research on the post-fire mechanical properties of Q460qENH weathering steel - particularly its mechanical behavior after exposure under different cooling methods - remains limited.

In the present study, experimental investigations were carried out to examine the post-fire mechanical behavior of Q460qENH weathering steel under three different cooling conditions. The microscopic damage mechanisms of the tensile fracture surfaces were analyzed using scanning electron microscopy (SEM), and the effects of fire exposure temperature and cooling method on the mechanical properties were systematically evaluated. Based on the experimental results, a mathematical model was developed to describe the relationship between mechanical behavior and fire exposure temperature under various cooling conditions. Furthermore, the post-fire mechanical properties of structural steels reported in previous studies were compiled and compared with the experimental data obtained in this work.

2. Test investigation

2.1. Materials and coupons

The Q460qENH weathering steel plate used in this study had a thickness of 10 mm and was manufactured by Nanjing Iron and Steel Co., Ltd. The chemical composition of the Q460qENH steel is presented in Table 1.

Table 1
The chemical composition of Q460qENH weathering steel (wt/%)

Chemical composition	C	Si	Mn	P	S	Ti	Cu	Cr	Ni
Content	0.07	0.26	1.4	0.012	0.002	0.012	0.29	0.48	0.29

The specimens were prepared in accordance with the GB/T 228.1 - 2021 standard [14]. The tensile loading direction was oriented perpendicular to the rolling direction of the steel plate. The geometry and dimensions of the specimens are illustrated in Fig. 1.

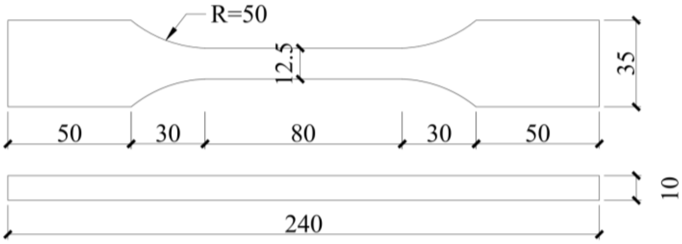

Fig. 1 Geometry of the specimens (mm)

2.2. Test setup

The experimental program consisted of three stages: heating, cooling, and room-temperature testing. The YTH-12-12 integrated muffle furnace was employed during the heating stage, as shown in Fig. 2(*a*). Nine specimens from each group were heated to target temperatures of 200 °C, 400 °C, 500 °C, 600 °C, 700 °C, 800 °C, 900 °C, and 1000 °C at a constant heating rate of 15 °C/min. The specimens were maintained at each target temperature for 30 minutes to ensure uniform thermal distribution. To investigate the effect of different cooling methods on the post-fire mechanical properties of Q460qENH weathering steel, the specimens were subjected to one of three cooling conditions immediately after removal from the furnace, as illustrated in Fig. 2. For the cooling in air (CIA) condition, specimens were placed on a stone platform and allowed to cool naturally to ambient temperature (approximately 25 °C). For the cooling in fire-fighting foam (CIF) condition, specimens were transferred to an open container, where aqueous film-forming foam (AFFF) was continuously sprayed until the foam completely submerged the specimens and no visible vapor remained. The foam-covered specimens were then left to cool beneath the insulating layer. For the cooling in water (CIW) condition, specimens were directly immersed in a water-filled container, removed upon reaching room temperature, and gently wiped dry.

(*a*) Integrated muffle furnace

(*b*) CIA

(*c*) CIW

(*d*) CIF

Fig. 2 Heating and cooling methods

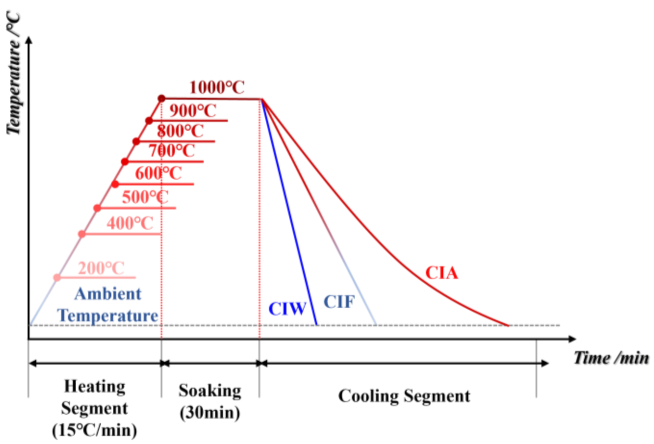

Fig. 3 Specimens heating and cooling curve

The cooling behavior associated with each method was also investigated. The time required for the specimens to cool from the target temperature to room temperature was recorded, and the average cooling rates for the CIA, CIF, and CIW conditions were approximately 1 °C/s, 5 °C/s, and 100 °C/s, respectively. It should be noted that these values represent average rates over the entire cooling process. In practice, the temperature evolution during cooling exhibits a nonlinear trend - characterized by a rapid initial decrease followed by a slower decline - consistent with the exponential decay patterns illustrated in Fig. 3.

To ensure the representativeness of the experimental results, three identical specimens were tested for each combination of target temperature (ranging from 200 °C to 1000 °C) and cooling method, resulting in a total of 72 high-temperature specimens (eight temperature levels and three cooling methods), along with three control specimens tested at room temperature (25 °C). Following the heating and cooling phases, monotonic tensile tests were performed at room temperature using a SANS SHT-600KN electro-hydraulic servo testing machine. The tests were conducted under displacement control at a loading rate of 1.5 mm/min, in accordance with the GB/T 228.1 - 2021 standard

[14]. Each test was continued until final fracture occurred. Tensile strain within the gauge section was measured using an 80 mm extensometer, and the corresponding data were recorded by the DCS - 200 data acquisition system. In addition, the effects of heating temperature and cooling method on the material hardness were evaluated through Brinell hardness measurements, performed using an HB-3000B testing instrument in compliance with GB/T 231.1 - 2018 [15]. The experimental setups are illustrated in Fig. 4.

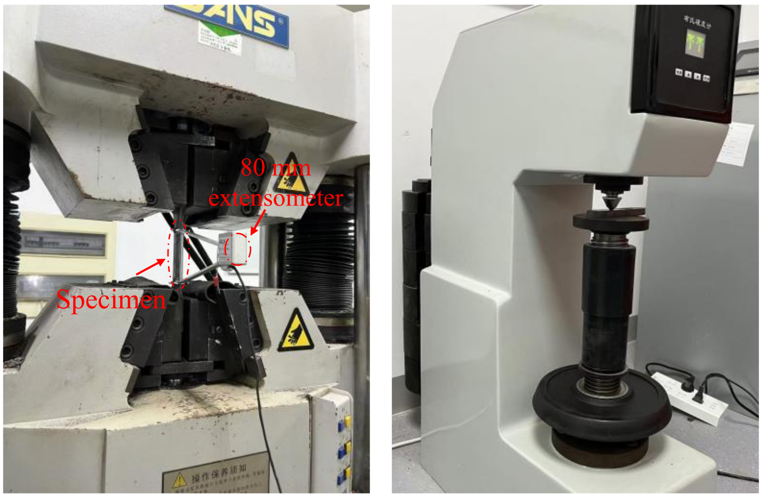

(*a*) Monotonic tensile test (*b*) Brinell hardness test

Fig. 4 Experimental setup

3. Test results

3.1. Visual observations

The post-fire surface appearance of Q460qENH weathering steel under the three cooling methods is illustrated in Fig. 5. For CIA specimens, a dark black oxide layer formed on the surface when the exposure temperature exceeded 600 °C, accompanied by partial spalling of the oxide layer. Correspondingly, the elongation after fracture increased. CIF specimens exhibited a tan surface color at exposure temperatures below 600 °C. As the temperature increased beyond 600 °C, the surface color gradually darkened to charcoal black. In these cases, the elongation after fracture showed minimal variation, except for the CIW1000 specimen. CIW specimens displayed a similar trend in surface color evolution to that observed in the CIF specimens.

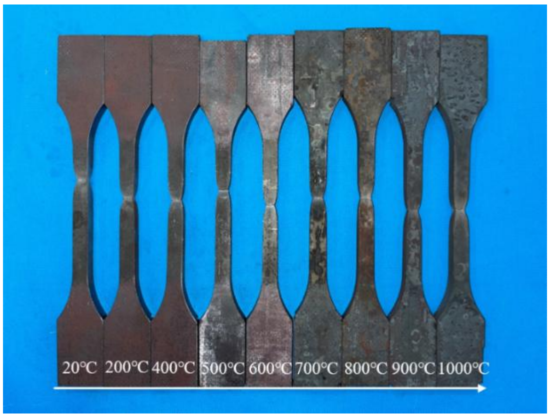

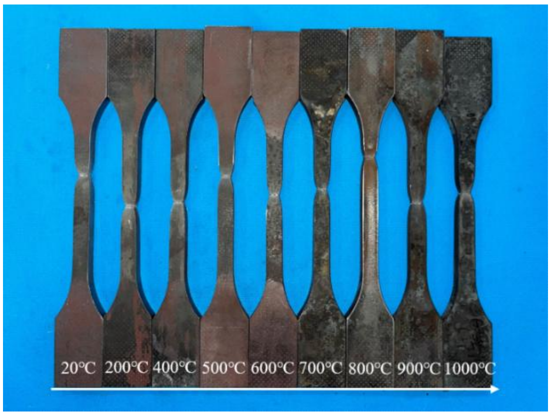

(*a*) CIA (*b*) CIF

(*c*) CIW

Fig. 5 Surface feature and failure patterns of specimens

The foam cooling method employed in this study utilized a 3% AFFF fire suppressant, which is a water-based agent primarily composed of fluorocarbon surfactants, hydrocarbon surfactants, solvents (e.g., glycol ethers), and foam stabilizers [16]. Upon contact with a high-temperature surface, the water component in the foam rapidly evaporates, resulting in intense localized heat absorption during the early stage of cooling. As cooling progresses, the foam forms a stable surface layer that significantly reduces the evaporation rate and insulates the specimen from ambient air. At this stage, heat dissipation occurs predominantly through conduction within the foam layer, while convective cooling is largely suppressed [17]. Consequently, the overall cooling efficiency gradually decreases, and the average cooling rate of CIF specimens over the full cooling period becomes comparable to that of CIA specimens, despite the higher initial heat extraction rate. This mechanism accounts for the similar mechanical properties observed under CIF and CIA conditions. It should also be noted that AFFF functions through a physical cooling process and does not chemically react with metallic materials such as steel during high-temperature exposure [18]. As shown in Fig. 5(*b*), no secondary chemical products resulting from interactions between the foam and the steel surface were observed.

3.2 Microfracture characteristics

The microfracture characteristics of specimens subjected to three different cooling methods were examined using a scanning electron microscope (SEM), as shown in Fig. 6. All fracture surfaces exhibited typical microvoid coalescence features, characterized by dimples of varying quantity, size, and depth. These dimples originated as microscopic voids formed during localized plastic deformation, with the fracture process comprising stages of void nucleation, growth, and coalescence. The consistent presence of dimple patterns is a fundamental indicator of ductile fracture mechanisms, and their areal fraction correlates directly with the material's ductility [19].

At the lower exposure temperature of 600 °C, the microfracture morphology exhibited only minor variations among the three cooling regimes. However, at elevated temperatures of 800 °C and 1000 °C, the influence of the cooling method became more pronounced, with distinct morphological features emerging under each condition. The CIA800 specimens displayed a dense distribution of deep dimples, indicating superior ductility. In contrast, the CIW800 specimens exhibited shallower and more sparsely distributed dimples, suggesting reduced plasticity. Similarly, the CIA1000 specimens revealed numerous dimples of varying sizes, whereas the CIF1000 specimens showed fewer dimples and a more uniform fracture surface. Notably, the CIW1000 specimens demonstrated a marked reduction in both the number and size of dimples, along with a smoother fracture surface, reflecting the pronounced effect of rapid water cooling on ductility degradation.

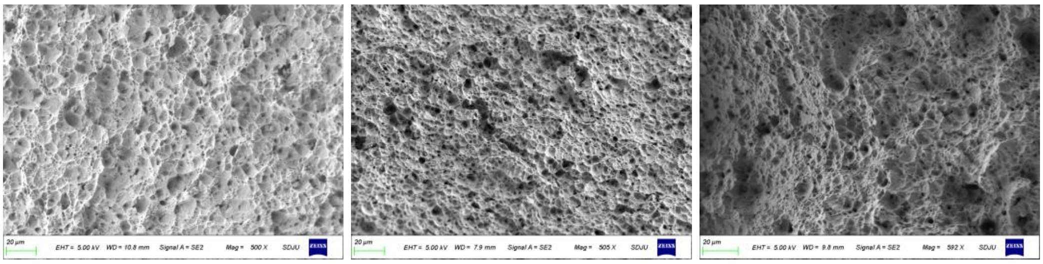

(*a*) CIA600 (*b*) CIA800 (*c*) CIA1000

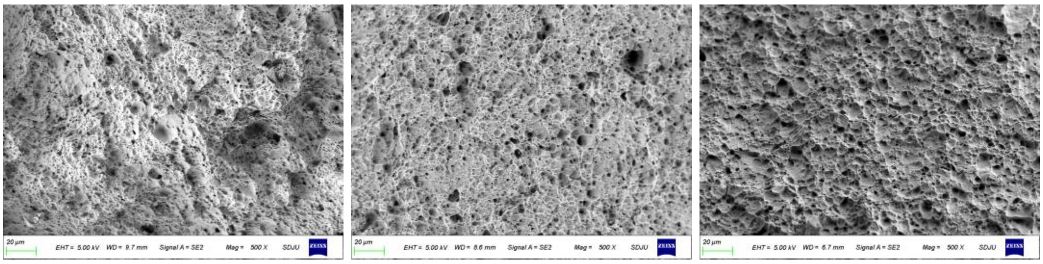

(*d*) CIF600 (*e*) CIF800 (*f*) CIF1000

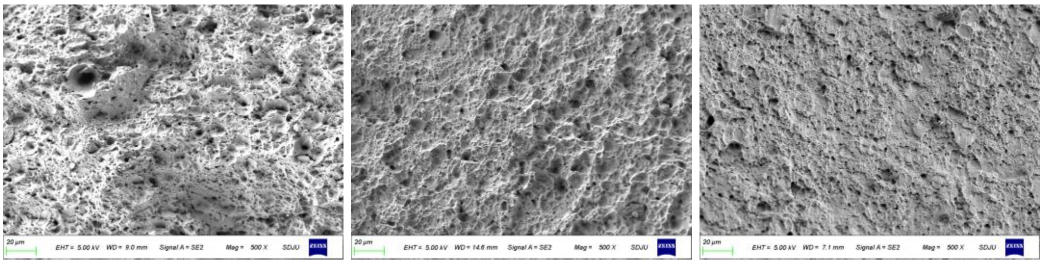

(*g*) CIW600 (*h*) CIW800 (*i*) CIW1000

Fig. 6 Microscopic fracture morphology

Although direct metallographic observations were not conducted in this study, it is well established that higher cooling rates promote the transformation of austenite into martensite, which enhances strength but reduces ductility [20]. In contrast, moderate cooling rates may lead to the formation of bainitic structures, while slower cooling facilitates the development of pearlite or a ferrite–pearlite mixture [21]. Furthermore, the observed evolution of fracture surface features qualitatively correlates with the temperature-dependent variation in elongation after fracture. For instance, specimens such as CIW800 and CIW1000, which exhibited smoother fracture surfaces with sparse and shallow dimples, also recorded significantly lower $\eta_{\varepsilon T}$ values. In comparison, the CIA800 and CIF800 specimens displayed denser and deeper dimples, consistent with their higher ductility. This qualitative agreement reinforces the established relationship between microscopic dimple morphology and macroscopic deformation capacity, as widely documented in ductile fracture studies [10,11,13,19].

4. Post-fire mechanical properties

4.1. Stress-strain curves

The stress - strain curves of Q460qENH weathering steel subjected to three different cooling methods after fire exposure are presented in Fig. 7.

Fig. 7 illustrates that at exposure temperatures up to 700 °C, the stress - strain curves of post-fire specimens remain closely aligned with those obtained under ambient conditions, exhibiting typical ductile failure behavior. Notably, the CIA700 and CIF700 specimens exhibit a pronounced reduction in yield strength compared to other cases, whereas the CIW700 specimens maintain a relatively stable yield strength. Q460qENH weathering steel displays a distinct yield plateau at lower temperatures (e.g., from room temperature to 600 °C), indicative of yield point elongation associated with strain aging and coordinated dislocation motion. However, as the exposure temperature increases - particularly beyond 800 °C - the yield plateau that is clearly visible at lower temperatures progressively disappears, and the material transitions from discontinuous to continuous yielding. This transformation reflects the microstructural reconstruction induced by high temperatures, including static recrystallization, dissolution of precipitates, and a reduction in dislocation density, which collectively diminish the yield delay mechanism [22,23]. Similar yielding behavior has been reported in other high-strength steels such as β-Ti alloy and Ti-5553 alloy, where the disappearance of the yield plateau serves as a useful indicator of thermal degradation and the evolution of deformation mechanisms [24,25]. While the ultimate strength remains largely unchanged for CIA and CIF specimens, a significant increase is observed in CIW specimens. These findings suggest that the mechanical properties of Q460qENH weathering steel undergo a transitional shift within the fire exposure temperature range of 700 °C to 800 °C, with the cooling method exerting a substantial influence on the nature of this mechanical transition.

Tables 2-4 summarize the post-fire mechanical properties of Q460qENH weathering steel under varying temperatures and cooling methods. A factor (η) is introduced to quantify the relative changes in mechanical parameters after high-temperature exposure. In Tables 2-4 ,η_E, η_{fy}, η_{fu}, η_{ET} and η_{EH} represent the ratios of post-fire test results to room-temperature test results for elastic modulus, yield strength, ultimate strength, elongation after fracture, and Brinell hardness, respectively. For stress-strain curves exhibiting a distinct yield plateau, the yield strength was defined as the lower yield point, and for curves without a yielding platform, the nominal yield strength was determined as the stress corresponding to 0.2% plastic strain.

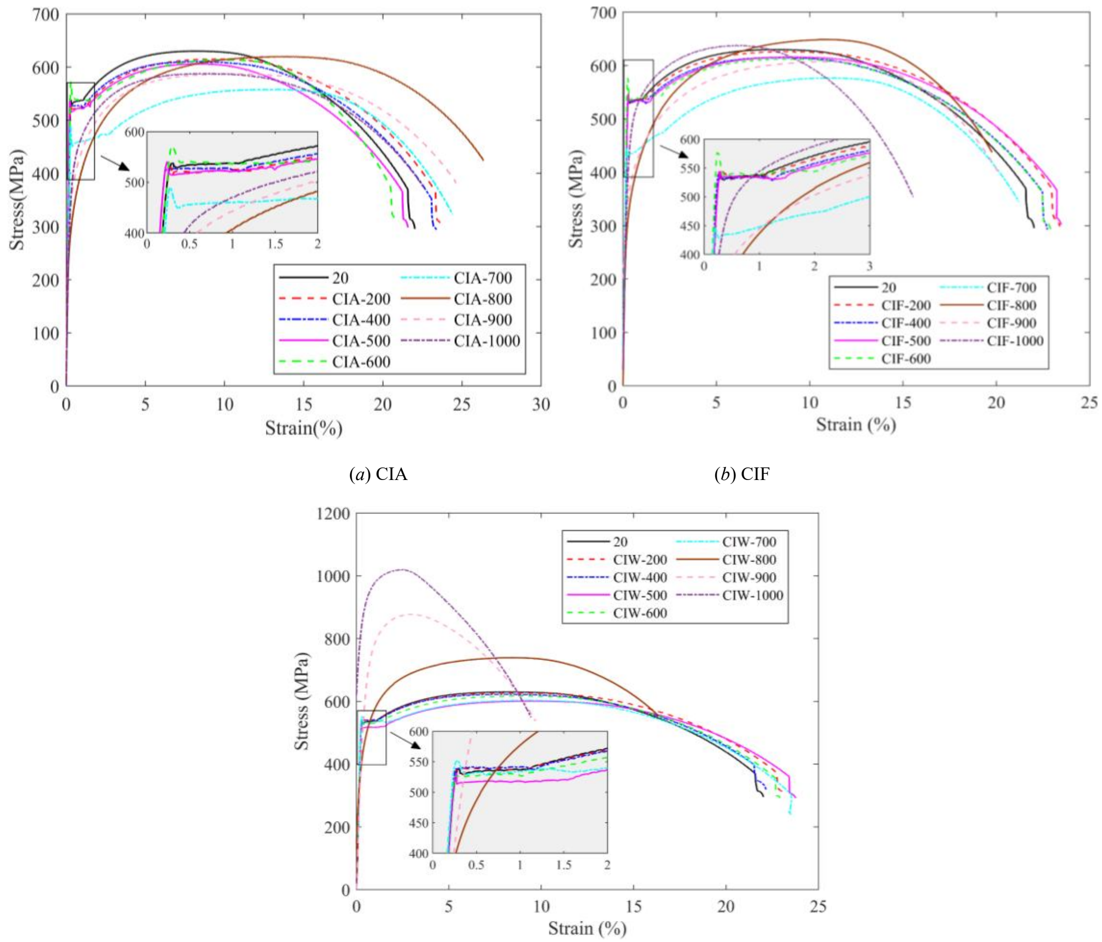

(*a*) CIA (*b*) CIF

(*c*) CIW

Fig. 7 Stress-strain relationships

Table 2
CIA test results (mean value)

Temperature (℃)	Elastic Modulus		Yield Strength		Ultimate Strength		Elongation after Fracture		Brinell Hardness	
	E/(GPa)	η_E	*fy*/(MPa)	η_{fy}	*fu*/(MPa)	η_{fu}	*εT*/(%)	$\eta_{εT}$	E_H/(HB)	η_{EH}
20	220.10 (11.63)	1.00	524.4 (11.16)	1.00	625.9 (9.39)	1.00	8.1 (0.06%)	1.00	194 (1.63)	1.00
200	222.20 (10.76)	1.01	518.9 (4.30)	0.99	619.8 (3.24)	0.99	7.9 (0.02%)	0.98	187 (1.41)	0.96
400	212.80 (10.09)	0.97	523.5 (4.68)	1.00	612.3 (2.48)	0.98	8.2 (0.31%)	1.01	198 (0.82)	1.02
500	217.65 (15.23)	0.99	513.5 (11.77)	0.98	603.6 (11.37)	0.96	7.5 (0.45%)	0.93	184 (1.41)	0.95
600	215.35 (11.18)	0.98	534.5 (2.86)	1.02	612.3 (6.21)	0.98	8.4 (0.67%)	1.04	182 (2.62)	0.94
700	208.15 (13.33)	0.95	444.0 (17.38)	0.85	579.9 (17.38)	0.93	9.3 (0.42%)	1.15	187 (0.82)	0.96
800	210.10 (11.40)	0.95	278.5 (2.78)	0.53	623.2 (6.09)	1.00	10.1 (0.08%)	1.25	180 (1.70)	0.93
900	227.90 (18.53)	1.04	312.1 (7.56)	0.60	588.6 (6.13)	0.94	9.5 (0.19%)	1.17	183 (2.05)	0.94
1000	205.65 (18.54)	0.93	347.8 (13.19)	0.66	587.9 (0.12)	0.94	8.1 (0.18%)	1.00	171 (4.19)	0.88

Note: The values in parentheses represent the standard deviation of the corresponding results

Table 3
CIF test results (mean value)

Temperature (℃)	Elastic Modulus		Yield Strength		Ultimate Strength		Elongation after Fracture		Brinell Hardness	
	E/(GPa)	η_E	fy/(MPa)	η_{fy}	fu/(MPa)	η_{fu}	εT/(%)	$\eta_{\varepsilon T}$	E_H/(HB)	η_{EH}
20	220.10 (11.64)	1.00	524.4 (11.16)	1.00	625.9 (9.39)	1.00	8.1 (0.06)	1.00	194 (1.63)	1.00
200	218.53 (7.58)	0.99	526.0 (8.95)	1.00	621.3 (9.35)	0.99	8.5 (1.00%)	1.05	186 (2.94)	0.96
400	214.50 (3.96)	0.97	524.7 (4.96)	1.00	613.9 (4.75)	0.98	7.9 (0.34%)	0.98	196 (3.30)	1.01
500	217.65 (7.75)	0.99	518.3 (9.62)	0.99	608.1 (5.90)	0.97	8.5 (0.41%)	1.05	194 (0.82)	1.00
600	233.20 (13.6)	1.06	531.6 (7.72)	1.01	610.1 (9.11)	0.97	7.6 (0.16%)	0.94	189 (1.89)	0.97
700	223.90 (7.42)	1.02	433.7 (19.47)	0.83	555.6 (17.86)	0.89	8.5 (0.45%)	1.05	197 (0.82)	1.02
800	207.40 (9.88)	0.94	371.8 (14.52)	0.71	643.0 (6.98)	1.03	8.6 (0.61%)	1.06	207 (2.16)	1.07
900	222.37 (13.95)	1.01	344.0 (13.63)	0.66	604.4 (3.38)	0.97	8.2 (0.38%)	1.01	187 (2.16)	0.96
1000	221.67 (16.19)	1.01	446.4 (13.22)	0.85	629.6 (8.46)	1.01	7.1 (0.86%)	0.88	200 (4.97)	1.03

Note: The values in parentheses represent the standard deviation of the corresponding results

Table 4
CIW test results (mean value)

Temperature (℃)	Elastic Modulus		Yield Strength		Ultimate Strength		Elongation after Fracture		Brinell Hardness	
	E/(GPa)	η_E	fy/(MPa)	η_{fy}	fu/(MPa)	η_{fu}	εT/(%)	$\eta_{\varepsilon T}$	HB	η_{HB}
20	220.10 (11.63)	1.00	524.4 (11.16)	1.00	625.9 (9.39)	1.00	8.1 (0.06%)	1.00	194 (1.63)	1.00
200	223.80 (15.63)	1.02	526.3 (5.84)	1.00	621.1 (5.06)	0.99	8.1 (0.20%)	1.00	193 (2.94)	0.99
400	216.60 (6.65)	0.98	526.6 (6.32)	1.00	615.4 (5.49)	0.98	7.5 (0.06%)	0.93	190 (3.56)	0.98
500	224.00 (17.46)	1.02	517.8 (12.15)	0.99	609.1 (11.77)	0.97	8.1 (0.14%)	1.00	199 (1.41)	1.03
600	227.87 (0.69)	1.04	524.2 (5.23)	1.00	614.3 (7.21)	0.98	8.0 (0.26%)	0.99	188 (2.05)	0.97
700	223.90 (17.27)	1.02	530.8 (7.03)	1.01	606.2 (7.15)	0.97	7.7 (0.43)	0.95	200 (2.16)	1.03
800	233.80 (11.02)	1.06	428.3 (10.56)	0.82	735.3 (16.73)	1.17	6.6 (0.87%)	0.81	199 (2.94)	1.03
900	211.75 (10.74)	0.96	703.5 (9.68)	1.34	923.7 (23.90)	1.48	4.9 (0.32%)	0.60	230 (6.38)	1.19
1000	228.05 (6.65)	1.04	793.7 (14.71)	1.51	983.4 (18.65)	1.57	4.3 (0.08%)	0.53	250 (4.32)	1.29

Note: The values in parentheses represent the standard deviation of the corresponding results

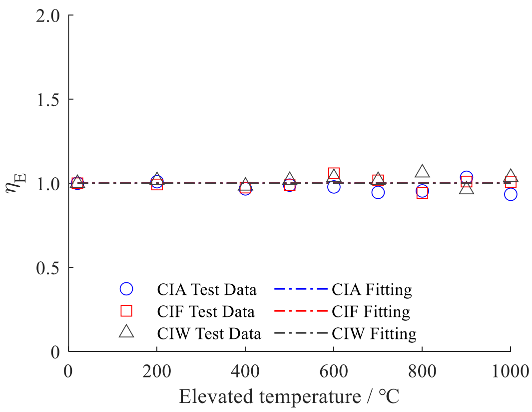

(*a*) Factor η_E versus fire exposure temperature

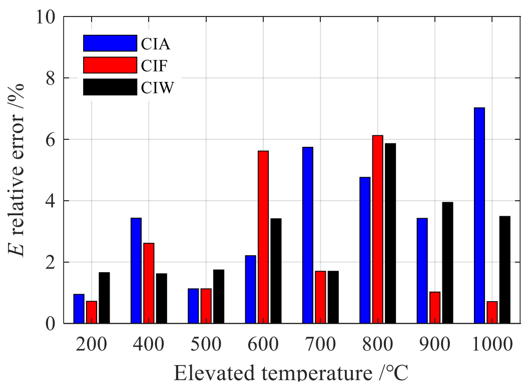

(*b*) Relative error

Fig. 8 Fitting results and prediction errors

4.2. Elastic modulus

The variation of the factor η_E with fire exposure temperature and the corresponding prediction error is illustrated in Fig. 8. The factor η_E exhibits only slight fluctuations under the three cooling methods, with standard deviations of 3.4%, 3.3%, and 3.1% for the CIA, CIF, and CIW conditions, respectively. These results indicate that the effects of exposure temperature and cooling rate on the elastic modulus of Q460qENH weathering steel are minimal, which is consistent with findings reported in previous studies [6,8,10-13].

As shown in Fig. 8(*b*), the relative prediction errors of the fitted equations under all three cooling methods are generally within 6.0%, with a maximum value of approximately 7.1% observed for the CIA condition at 1000 °C. The overall trend indicates that the prediction error tends to increase with rising temperature, particularly under the cooling-in-air condition. Nevertheless, the relatively low and stable error magnitudes across all temperature levels and cooling methods further demonstrate the reliability and robustness of the proposed prediction model for η_E.

4.3. Yield strength

The variation of the factor η_{fy} with fire exposure temperature is illustrated in Fig. 9(*a*). When the post-fire temperature is below 600 °C, η_{fy} ranges from 0.98 to 1.02 under the CIA condition and from 0.99 to 1.01 under the CIF condition. However, as the exposure temperature increases from 700 °C to 1000 °C, the post-fire yield strength of Q460qENH weathering steel exhibits a decreasing trend followed by a recovery. Consequently, the temperature transition point for mechanical properties can be identified at approximately 600 °C for both CIA and CIF conditions. Specifically, for CIA specimens, η_{fy} reaches its minimum value of 0.53 at 800 °C and then recovers to 0.66 at 1000 °C. Similarly, CIF specimens show a minimum η_{fy} of 0.66 at 800 °C, followed by a rebound to 0.85 at 1000 °C. These results indicate that after high-temperature exposure, the effect of CIF on yield strength is less pronounced than that of CIA, which can be attributed to the slightly higher cooling rate under CIF compared with CIA.

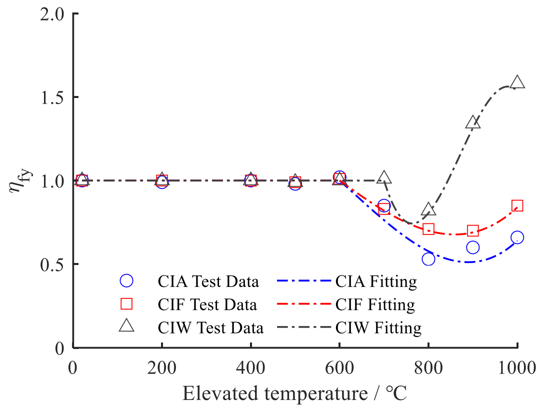

(*a*) Factor η_{fy} versus fire exposure temperature

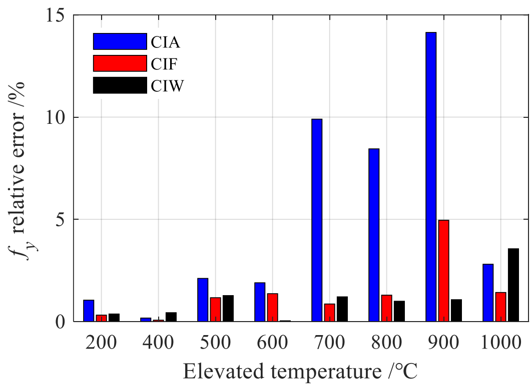

(*b*) Relative error

Fig. 9 Fitting results and prediction errors

The temperature transition point for the CIW condition is determined to be 700 °C, as η_{fy} at this exposure temperature equals 1.01, indicating no significant change in post-fire yield strength compared with room-temperature specimens. At 800 °C, the post-fire yield strength of the CIW800 specimen decreases by 18.0% relative to room temperature. However, as the temperature further increases, η_{fy} sharply rises to 1.34 and 1.51 for CIW900 and CIW1000, respectively.

Based on the variation of η_{fy} under the CIA, CIF, and CIW conditions for Q460qENH weathering steel, cubic polynomial fitting was employed to establish predictive equations, as shown in Eqs. (1) - (3). As illustrated in Fig. 9(*b*), the fitted models exhibit satisfactory accuracy, with most relative prediction errors remaining below 10% and the maximum error not exceeding 14.2%. These results confirm the reliability and robustness of the proposed equations across different high-temperature exposures and cooling methods.

Prediction of variation factor $\eta_{fy,\,CIA}$ for CIA (R^2=0.92):

$$\eta_{fy,\,CIA}=\frac{f_{y,\,T}}{f_{y,20}}=\begin{cases}1 & 20°C\le T\le 600°C\\ 2.52\left(\frac{T}{600}-1\right)^3-0.33\left(\frac{T}{600}-1\right)^2-1.44\left(\frac{T}{600}-1\right)+1 & 600°C<T\le 1000°C\end{cases}\quad(1)$$

Prediction of variation factor $\eta_{fy,\,CIF}$ for CIF (R^2=0.98):

$$\eta_{fy,\,CIF}=\frac{f_{y,\,T}}{f_{y,20}}=\begin{cases}1 & 20°C\le T\le 600°C\\ 1.80\left(\frac{T}{600}-1\right)^3+0.18\left(\frac{T}{600}-1\right)^2-1.16\left(\frac{T}{600}-1\right)+1 & 600°C<T\le 1000°C\end{cases}\quad(2)$$

Prediction of variation factor $\eta_{fy,\,CIW}$ for CIW (R^2=0.98):

$$\eta_{fy,\,CIW}=\frac{f_{y,\,T}}{f_{y,20}}=\begin{cases}1 & 20°C\le T\le 700°C\\ -56.59\left(\frac{T}{700}-1\right)^3+41.65\left(\frac{T}{700}-1\right)^2-6.13\left(\frac{T}{700}-1\right)+1 & 700°C<T\le 1000°C\end{cases}\quad(3)$$

4.4. Ultimate strength

The variation of the factor η_{fu} with fire exposure temperature is illustrated in Fig. 10(*a*). It is evident that under both CIA and CIF conditions, the influence of elevated temperature exposure on the post-fire ultimate strength is negligible.

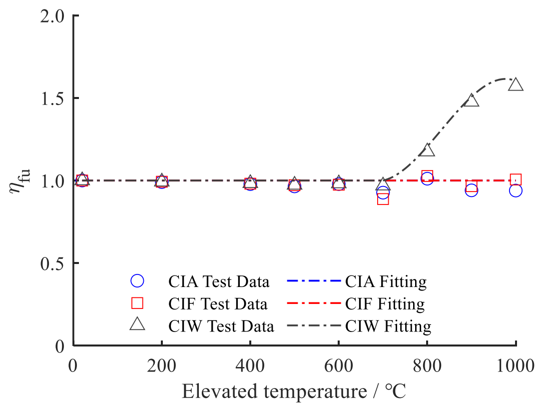

(*a*) Factor η_{fu} versus fire exposure temperature

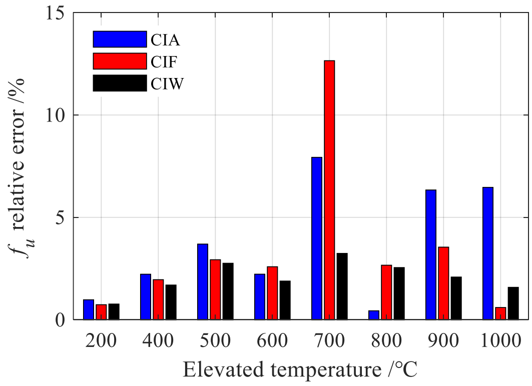

(*b*) Relative error

Fig.10 Fitting results and prediction errors

For the CIW condition, when the exposure temperature remains below the transition point of 700 °C, the post-fire ultimate strength of Q460qENH weathering steel remains largely unchanged. However, once the exposure temperature exceeds this transition point, the post-fire ultimate strength exhibits a pronounced increase, reaching values of 1.17, 1.48, and 1.57 for the CIW800, CIW900, and CIW1000 specimens, respectively. Moreover, the relative prediction errors shown in Fig. 10(*b*) confirm the satisfactory accuracy of the fitted model for η_{fu}. Across all temperature levels, most error values remain below 10%, with slightly higher deviations observed near the transition temperature region. These results demonstrate that the proposed model effectively captures the temperature-dependent variation in post-fire ultimate strength, particularly under the CIW condition. A mathematical model describing the variation in the post-fire ultimate strength of Q460qENH weathering steel under the CIW condition is presented in Eq. (4).

Prediction of variation factor $\eta_{fu,\,CIW}$ for CIW (R^2=0.92):

$$\eta_{fu,\ CIW}=\frac{f_{u,\ T}}{f_{u,20}}=\begin{cases}1 & 20°C\le T\le 700°C\\ -17.19\left(\frac{T}{700}-1\right)^3+9.69\left(\frac{T}{700}-1\right)^2+0.41\left(\frac{T}{700}-1\right)+1 & 700°C<T\le 1000°C\end{cases} \quad (4)$$

4.5. *Elongation after fracture*

The ductility of steel after fire exposure can be evaluated by examining the reduction in elongation after fracture. This parameter represents the percentage change in elongation relative to the specimen's original length, serving as a quantitative indicator of its deformation capacity prior to failure. The factor $\eta_{\varepsilon T}$, which characterizes the post-fire elongation after fracture under the three cooling methods, is compared in Fig. 11(*a*).

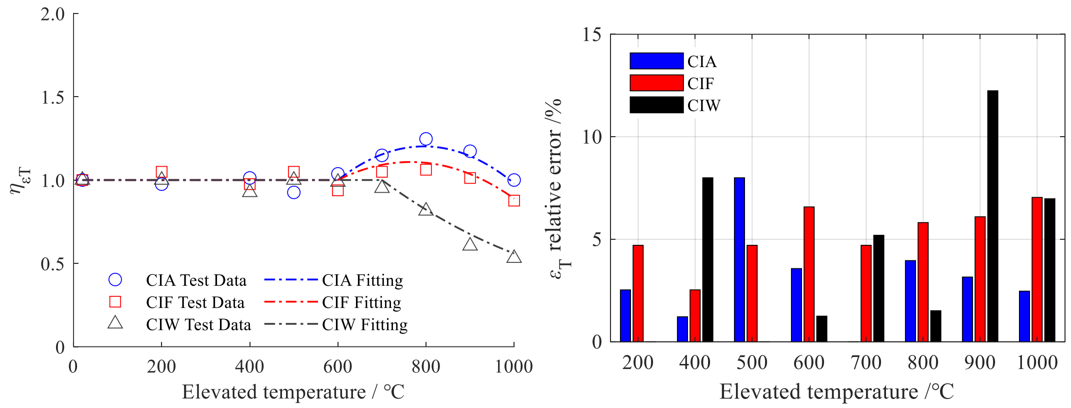

(*a*) Factor $\eta_{\varepsilon T}$ versus fire exposure temperature (*b*) Relative error

Fig. 11 Fitting results and prediction errors

For all three cooling methods, the effect of elevated temperature exposure on elongation after fracture is negligible below their respective temperature transition points. When the exposure temperature exceeds the transition point of 600 °C for the CIA and CIF specimens, the elongation after fracture initially increases and then decreases. Specifically, it reaches peak values of 1.25 and 1.06 for the CIA and CIF specimens at 800 °C, respectively, and subsequently decreases to approximately 1.00 and 0.88 at 1000 °C. In contrast, for the CIW specimens, once the exposure temperature exceeds the transition point of 700 °C, the factor $\eta_{\varepsilon T}$ undergoes a significant decline, reaching a minimum value of 0.53 at an exposure temperature of 1000 °C. The fitted equations for the factor $\eta_{\varepsilon T}$ under the different cooling methods are provided in Eqs. (5)-(7).

As shown in Fig. 11(*b*), the relative prediction errors for $\eta_{\varepsilon T}$ vary with temperature and cooling method. For the CIA specimens, the errors remain below 8.0% at all temperatures. The CIF specimens exhibit relatively stable deviations across the entire temperature range, with a maximum error of approximately 7.1%. Under the CIW condition, slightly higher deviations are observed, reaching a peak error of 12.2% at 900 °C. These results indicate that the fitted models capture the temperature-dependent post-fire elongation after fracture behavior with satisfactory accuracy across all cooling scenarios.

Prediction of variation factor $\eta_{\varepsilon T,\,CIA}$ for CIA (R^2=0.96):

$$\eta_{\varepsilon T,\ CIA}=\frac{\varepsilon_{T,\ T}}{\varepsilon_{T,20}}=\begin{cases}1 & 20°C\le T\le 600°C\\ -1.91\left(\frac{T}{600}-1\right)^2+1.24\left(\frac{T}{600}-1\right)+1 & 600°C<T\le 1000°C\end{cases} \quad (5)$$

Prediction of variation factor $\eta_{\varepsilon T,\,CIF}$ for CIF (R^2=0.92):

$$\eta_{\varepsilon T,\ CIF}=\frac{\varepsilon_{T,\ T}}{\varepsilon_{T,20}}=\begin{cases}1 & 20°C\le T\le 600°C\\ -1.43\left(\frac{T}{600}-1\right)^2+0.86\left(\frac{T}{600}-1\right)+1 & 600°C<T\le 1000°C\end{cases} \quad (6)$$

Prediction of variation factor $\eta_{\varepsilon T,\,CIW}$ for CIW (R^2=0.98):

$$\eta_{\varepsilon T,\ CIW}=\frac{\varepsilon_{T,\ T}}{\varepsilon_{T,20}}=\begin{cases}1 & 20°C\le T\le 700°C\\ 0.76\left(\frac{T}{600}-1\right)^2-1.35\left(\frac{T}{600}-1\right)+1 & 700°C<T\le 1000°C\end{cases} \quad (7)$$

4.6. *Brinell hardness*

Hardness serves as a critical indicator for evaluating the mechanical properties of metallic materials, representing their resistance to localized deformation—particularly plastic deformation, indentation, and scratching-under static loading conditions. Materials with higher hardness typically demonstrate superior wear resistance, and this parameter reflects, to some extent, the overall mechanical performance of the material. A well-established correlation exists between Brinell hardness and other mechanical properties, such as ultimate tensile strength [26]. Consequently, hardness testing provides a valuable, non-destructive means of indirectly assessing material strength, particularly in scenarios where destructive testing is impractical. However, studies focusing on the post-fire hardness characteristics of structural steels remain relatively limited.

The pronounced increase in strength and Brinell hardness, along with the significant reduction in elongation observed in the CIW800 - 1000 specimens, suggests a notable microstructural transition induced by rapid water cooling from elevated temperatures. When high-strength steels are cooled rapidly from the austenitic range, martensitic transformation tends to occur, typically characterized by a high dislocation density, refined lath structures, and elevated internal strain energy-features that contribute to increased mechanical strength and hardness [27]. In this study, the CIW specimens subjected to cooling from 800 °C and above exhibited more than a 20% increase in hardness, accompanied by marked changes in fracture morphology - such as reduced dimple size, smoother fracture surfaces, and lower ductility indices - as shown in Figs. 6(*h*), 6(*i*), and 11(*a*). These trends are consistent with the characteristics of martensitic transformation reported in previous studies on fire-exposed steels undergoing rapid quenching [20,21], indicating that phase transformation likely governs the observed mechanical behavior. Fig. 12 illustrates the variation of the η_{HB} factor for Q460qENH weathering steel as a function of fire exposure temperature and prediction error.

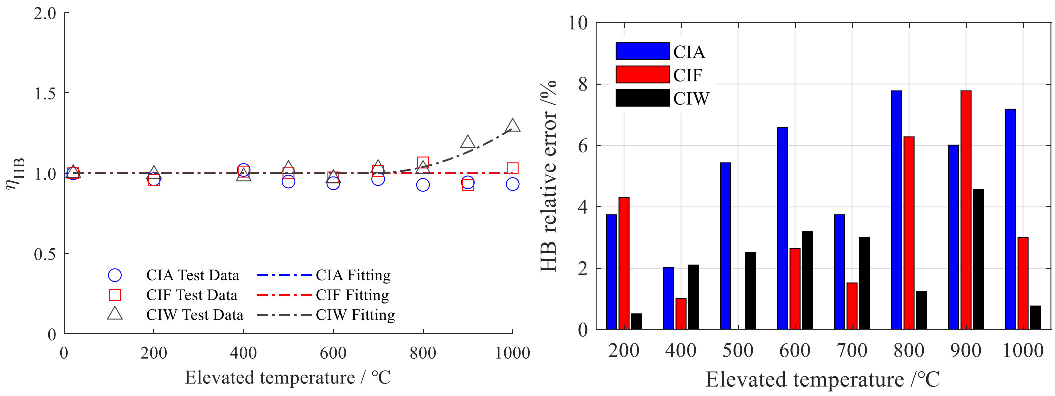

(*a*) Factor η_{HB} versus fire exposure temperature (*b*) Relative error

Fig. 12 Fitting results and prediction errors

The results demonstrate that under both CIA and CIF conditions, elevated temperature exposure has minimal influence on post-fire Brinell hardness. In contrast, under the CIW condition, a significant increase in Brinell hardness is observed once the exposure temperature exceeds the transition point of 700 °C. Specifically, compared with the room-temperature values, the Brinell hardness increases by 2.6%, 18.6%, and 28.9% at exposure temperatures of 800 °C, 900 °C, and 1000 °C, respectively. This phenomenon can be attributed to the accelerated cooling rate above 700 °C, which promotes martensitic transformation in the weathering steel and leads to a substantial enhancement in hardness during water cooling [27]. As shown in Fig. 12(*b*), the relative prediction errors for η_{HB} vary with both temperature and cooling method. Under the CIA and CIF conditions, the errors range from 1.0% to 7.8%, with the largest deviations occurring at 800 °C and 900 °C, respectively. In contrast, the CIW condition exhibits lower overall errors, mostly below 4.6%, reaching as low as 0.8% at 1000 °C. These results indicate that the prediction model performs well across all conditions, exhibiting particularly stable accuracy under the CIW regime. Based on these observations, a mathematical model describing the variation of Brinell hardness for Q460qENH weathering steel under the CIW condition is proposed in Eq. (8).

Prediction of variation factor $\eta_{HB,\,CIW}$ for CIW (R^2=0.95):

$$\eta_{HB,CIW}=\frac{HB_{,T}}{HB_{,20}}=\begin{cases}1 & 20°C \le T \le 700°C \\ 1.33\left(\frac{T}{700}-1\right)^2+0.08\left(\frac{T}{700}-1\right)+1 & 700°C < T \le 1000°C\end{cases} \tag{8}$$

These predictive equations, established based on statistically averaged results from three specimens per condition, demonstrate good accuracy, with relative errors mostly within 15.0% across all temperature levels and cooling regimes, as illustrated in Figs. 8-12. Their robustness and low prediction deviations confirm their reliability for practical applications. Moreover, the equations cover a wide range of fire exposure temperatures (200 °C to 1000 °C) and account for three representative cooling conditions - cooling in air, cooling in foam, and cooling in water - thus providing a flexible and versatile toolset for post-fire performance evaluation.

5. Comparisons and discussion

This section presents a comparative analysis of the mechanical properties of Q460qENH weathering steel and other steel grades after fire exposure. Table 5 summarizes the steel grades and corresponding test conditions reported in the literature, focusing on the comparison of key mechanical property parameters, including elastic modulus, yield strength, and ultimate strength.

Table 5
Comparison of mechanical properties of different steel grades

Steel Grade	Source	Heating Temperature (°C)	Cooling method	Cross section shape
Q235	Lu [28]	100~1000	CIA, CIW	Rectangle
Q345	Lu [28]	100~1000	CIA, CIW	Rectangle
Q345	Zhang [13]	200~900	CIF	Rectangle
Q355	Zhang [11]	200~900	CIF, CIW	Rectangle
Q355qNH	Zhang [5]	300~1000	CIA, CIW	Rectangle
Q420	Lu [28]	100~1000	CIA, CIW	Rectangle
Q460	Zhang [19]	200~900	CIF	Rectangle
Q460	Wang [29]	300~900	CIA, CIW	Rectangle
Q550	Song [30]	200~900	CIA, CIW	Rectangle
Q620	Zhou [12]	300~900	CIA, CIF, CIW	Rectangle
Q690	Zhang [19]	200~900	CIF	Rectangle
Q690	Li [31]	300~900	CIA, CIW	Rectangle
Q890	Zeng [32]	200~1000	CIA, CIW	Rectangle
Q960	Wang [33]	300~900	CIA, CIW	Circular
S460	Qiang [34]	300~1000	CIA	Rectangle
S690	Qiang [34]	100~1000	CIA	Rectangle
S960	Qiang [8]	300~1000	CIA	Rectangle
A36	Sajid [27]	500~1000	CIA, CIW	Hollow Circular
A572	Sajid [35]	500~1000	CIA, CIW	Hollow Circular
A992	LEE J [36]	200~1000	CIA, CIW	Rectangle

Fig. 13 illustrates the variation in the elastic modulus of various steels with increasing fire-exposure temperature under different cooling conditions. Under the CIA condition, for Q960, S460, S690, and S960 steels, when the fire-exposure temperature exceeds 600 °C, the elastic modulus decreases significantly, indicating a notable degradation in the mechanical properties of these steels under high-temperature conditions. However, for the remaining steels, the elastic modulus exhibits only minor fluctuations, with a variation range of -14.0% to 7.0%. Similarly, under the CIF condition, the elastic modulus of Q460qENH and the other steels remains stable with increasing fire-exposure temperature, exhibiting only slight variations across the entire temperature range. Under the CIW condition, as the fire-exposure temperature increases, the elastic modulus of each steel generally shows a slight downward trend, though the overall variation range remains small. Notably, at a fire-exposure temperature of 1000 °C, the CIA1000 specimen exhibits an η_E of 0.93, while the CIW1000 specimen shows an η_E of 1.04, both indicating good stability of the elastic modulus after high-temperature cooling.

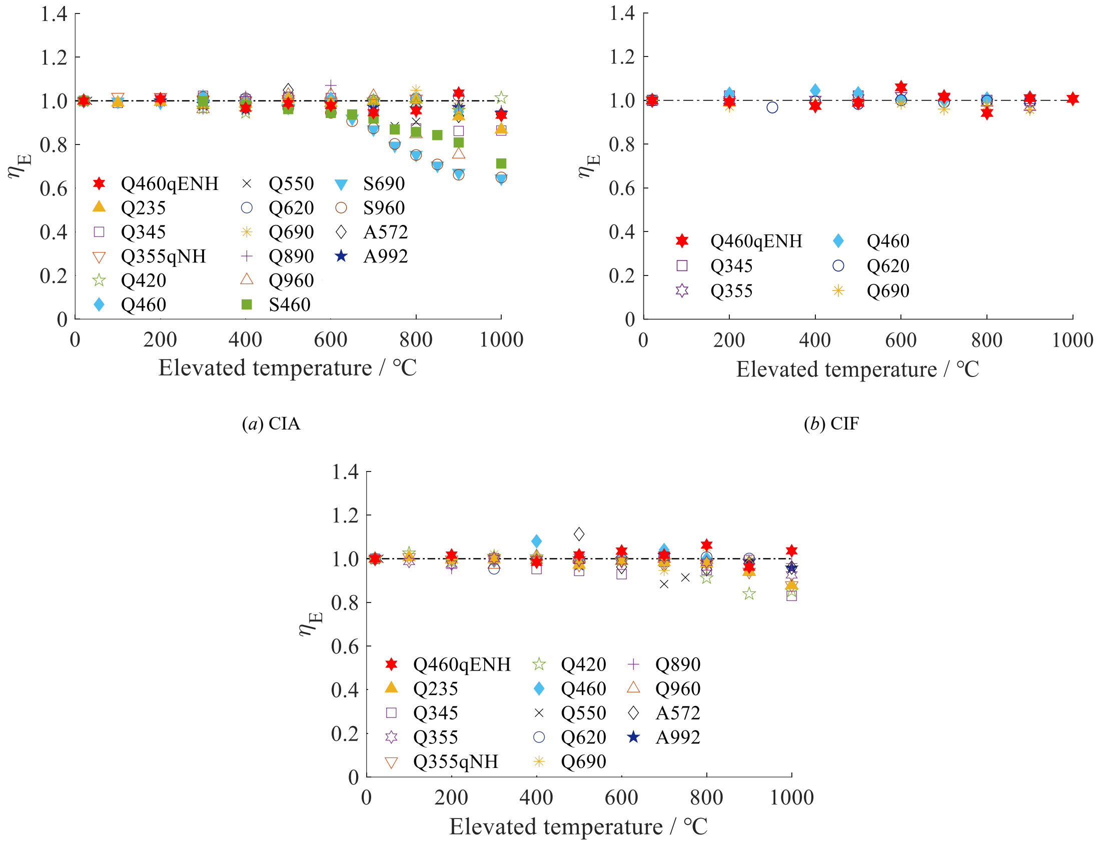

(*a*) CIA

(*b*) CIF

(*c*) CIW

Fig. 13 Comparison on post-fire elastic modulus

Fig. 14 presents a comparison of the post-fire yield strength of different steel grades. When the fire-exposure temperature exceeds 800 °C, both Q460qENH and Q960 steels exhibit strength recovery, with their η_{fy} increasing by 13% and 16%, respectively. Except for Q235 and Q345 steels, the yield strength of other steels increases following water cooling at temperatures above 800 °C. Specifically, after exposure to a high temperature of 900 °C, the yield strengths of A36 and A572 steels under CIW conditions are 143% and 103% higher, respectively, than those under CIA conditions. Microstructural analysis indicates that this phenomenon is attributed to the transformation of high-temperature austenite into ferrite and the strengthening phase, martensite, resulting from water cooling [37,38]. According to the evaluation code T/CECS 252:2019 [39], under the CIA condition, the yield strength of Q460qENH weathering steel meets the code requirements when the fire-exposure temperature is below 600 °C. However, when the temperature exceeds 600 °C, the yield strengths of Q550, Q620, Q690, Q890, Q960, S690, S960, and A572 steels decrease significantly, with reductions exceeding the allowable limits specified by the code. Under the CIF condition, the post-fire yield strength of most steels shows a trend consistent with that observed under CIA conditions. Notably, high-strength steels such as Q460, Q620, and Q690 exhibit moderate reductions in yield strength when the fire-exposure temperature exceeds 700 °C. These results suggest that although foam cooling provides faster initial heat extraction, its subsequent insulating effect slows the overall cooling process, resulting in thermal histories that closely resemble those of natural air cooling. Consequently, the mechanical degradation patterns under CIF and CIA conditions tend to converge.

Fig. 15 presents a comparison of the post-fire ultimate strength of different steel grades. The results indicate that under CIA conditions, the post-fire strength of Q460qENH weathering steel and A992 steel, after exposure to various high temperatures, still satisfies the strength requirements specified in GB/T 19879-2023 [40]. For the other steels, once the fire-exposure temperature exceeds the critical threshold, the ultimate strength falls below the lower limit defined by the standard. Under CIF conditions, with the exception of Q460qENH weathering steel, all other tested steel grades exhibit varying degrees of post-fire degradation in ultimate strength when the exposure temperature exceeds 700 °C. Notably, for Q460, Q620, and Q690 steels, the ultimate strength decreases by approximately 30% after exposure to 900 °C. This degradation trend under CIF conditions closely resembles that observed under CIA. However, the slightly improved strength retention observed under CIF suggests that foam cooling may provide a modest thermal-buffering effect, mitigating the extent of high-temperature damage compared with natural air cooling. Under CIW conditions, the ultimate strength of each steel generally follows the same trend as its yield strength. When the temperature exceeds 700 °C, the ultimate strength of A36 and A572 steels increases significantly, with the factor η_{fu} rising by 154% and 102%, respectively, after exposure to 900 °C. Notably, under CIW conditions, the ultimate strength of Q460qENH weathering steel increases by 60% following exposure to 1000 °C, indicating exceptional post-fire strengthening behavior under rapid water quenching.

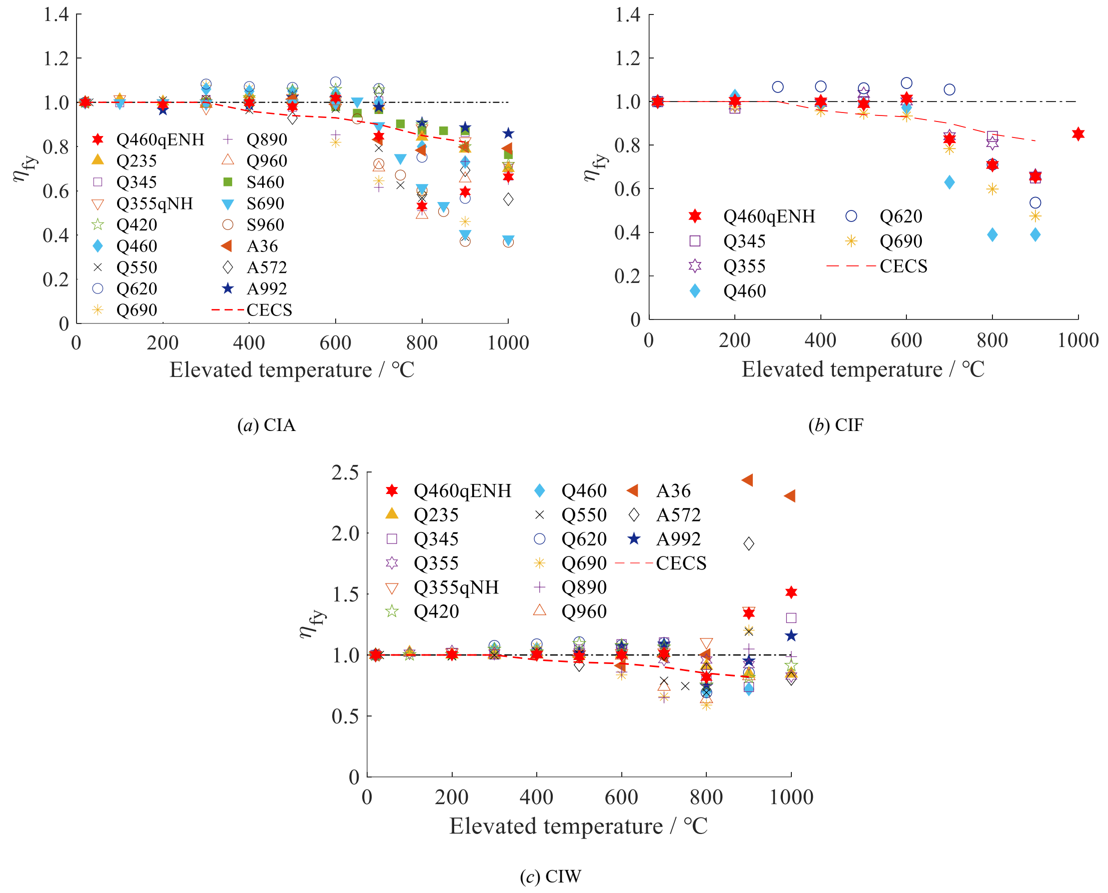

Fig. 14 Comparison on post-fire yield strength

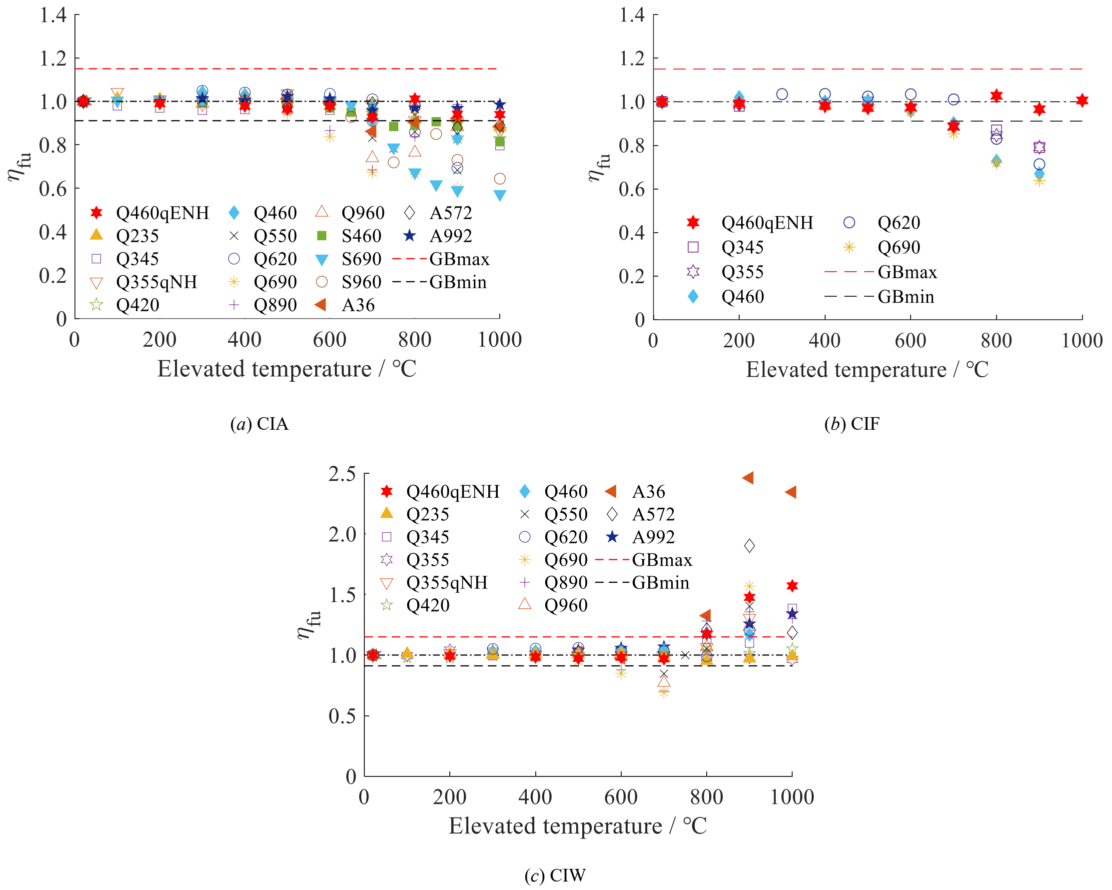

Fig. 15 Comparison on post-fire ultimate strength

Based on the comparative analysis of the experimental data, Q460qENH weathering steel exhibits outstanding post-fire mechanical performance under both CIA and CIW conditions. These results establish a solid foundation for evaluating the residual mechanical properties of weathering steel after fire exposure. Furthermore, the proposed predictive models, which correlate temperature with key mechanical parameters, not only facilitate the quantitative assessment of performance degradation but also provide valuable theoretical support for the development and refinement of fire-resistant design standards for steel structures.

6. Conclusions

(1) After exposure to elevated temperatures, Q460qENH weathering steel exhibits notable changes in both surface morphology and microstructure, depending on the applied cooling method. The resulting surface characteristics serve as indicators of the thermal history and cooling conditions experienced by the steel. Microstructural observations suggest that water immersion cooling (CIW) leads to a pronounced reduction in material toughness, underscoring the sensitivity of Q460qENH to rapid quenching effects.

(2) The phase transformation temperature for the CIA and CIF specimens is identified as 600 °C. Below this threshold, all mechanical properties remain stable. However, when the temperature exceeds 600 °C, the elastic modulus, ultimate tensile strength, and Brinell hardness exhibit only minor variations, whereas the yield strength and elongation after fracture change significantly. For the CIW specimens, the phase transformation temperature is determined to be 700 °C, above which all mechanical properties undergo pronounced changes.

(3) A comparative investigation was conducted between Q460qENH weathering steel and other types of steel, categorized as low-carbon steel (e.g., Q235, A36), mild steel (e.g., Q345, Q355, Q355qNH), and high-strength steel (e.g., Q420, Q460, Q550, Q620, Q690, Q890, Q960, S460, S690, S960, A572, A992), to evaluate the post-fire mechanical performance of Q460qENH. The results indicate that Q460qENH exhibits excellent fire resistance.

Availability of data and materials

The data that support the findings of this study are available from the corresponding author upon reasonable request.

Disclosure Statement

No potential conflict of interest was reported by the author(s).

Funding

This work was supported by Major Scientific & Technological Innovation Projects of Shandong Province, P. R. China (No. 2021CXGC011204)

References

[1] Juan José Pagán-Martínez, Ignacio Paya-Zaforteza, Antonio Hospitaler-Pérez. Post-fire assessment of composite steel-concrete box-girder bridges: Lessons from a recent incident[J]. Journal of Constructional Steel Research, 2024, 214:108425.

[2] Gang Zhang, Xiaocui Zhao, Zelei Lu, et al. Review and discussion on fire behavior of bridge girders[J]. Journal of Traffic and Transportation Engineering (English Edition), 2022, 9(3):422-446.

[3] Jiayu Hu, Ricky Carvel, Asif Usmani. Bridge fires in the 21st century: A literature review[J]. Fire Safety Journal, 2021, 126:103487.

[4] Santosh Timilsina, Nur Yazdani, Eyosias Beneberu. Post-fire analysis and numerical modeling of a fire-damaged concrete bridge[J]. Engineering Structures, 2021, 244:112764.

[5] Xin Zhang, Hang Yin, Ernian Zhao, Jinhui Liu. Experiment on Post-fire Mechanical Properties of Q355qNH Bridge Weathering Steel. Materials Reports, 2023, 37(23): 22050150-6.

[6] Linxin Song, Guoqiang Li. Processing and cooling effects on post-fire mechanical properties of high strength structural steels[J]. Fire Safety Journal, 2021, 122: 103346.

[7] Fang Wang, Lui E M. Experimental study of the post-fire mechanical properties of Q690 high strength steel[J]. Journal of Constructional Steel Research, 2020, 167: 105966.

[8] Xuhong Qiang, Frans S.K. Bijlaard, Henk Kolstein. Post-fire performance of very high strength steel S960[J]. Journal of Constructional Steel Research, 2013, 80:235-242.

[9] Haiting Li, Ben Young. Residual mechanical properties of high strength steels after exposure to fire[J]. Journal of Constructional Steel Research, 2018, 148:562-571.

[10] Chong Ren, Liusi Dai, Yuner Huang, et al. Experimental investigation of post-fire mechanical properties of Q235 cold-formed steel[J]. Thin-Walled Structures, 2020, 150: 106651.

[11] Chuntao Zhang, Bin Jia, Junjie Wang. Influence of artificial cooling methods on post-fire mechanical properties of Q355 structural steel[J]. Construction and Building Materials, 2020, 252:119092.

[12] Xuhong Zhou, Xuanyi Xue, Yu Shi, et al. Post-fire mechanical properties of Q620 high-strength steel with different cooling methods[J]. Journal of Constructional Steel Research, 2021, 180: 106608.

[13] Chuntao Zhang, Meiqi Gong, Li Zhu. Post-fire mechanical behavior of Q345 structural steel after repeated cooling from elevated temperatures with fire-extinguishing foam[J]. Journal of Constructional Steel Research, 2022, 191: 107201.

[14] GB/T 228.1–2021, Metallic Materials-Tensile Testing-Part 1: Method of Test at Room Temperature, China Standard Press, Beijing, China, 2021.

[15] GB/T 231.1-2018, Metallic Materials-Brinell Hardness Test-Part 1: Test Method, China Standard Press, Beijing, China, 2018.

[16] GB/T 50151–2021, Technical Standard for Foam Extinguishing Systems, China Planning Publishing House, Beijing, China, 2021.

[17] Tao Chen, Peng Zhang, Dezheng Wang, et al. Research on Suppression Effect of Low-Expansion AFFF, AFFF/AR and FFFP Foam on Hot Oil Fire for Oil-Immersed Transformers[J]. Thermal Science and Engineering Progress, 2023.

[18] Youjie Sheng, Menghua Xue, Li Ma, et al. Environmentally Friendly Firefighting Foams Used to Fight Flammable Liquid Fire[J]. Fire Technology, 2021(7).

[19] Chuntao Zhang, Ruheng Wang, Gangbing Song. Post-fire mechanical properties of Q460 and Q690 high strength steels after fire-fighting foam cooling[J]. Thin-Walled Structures, 2020, 156: 106983.

[20] Guofang Liang, Qiyang Tan, Yingang Liu, et al. Effect of cooling rate on microstructure and mechanical properties of a low-carbon low-alloy steel[J]. Journal of Materials Science, 2021, 56(5):1-11.

[21] Hinton J S , Palmiere E J , Mark R W .Effect of Cooling Rate on the Room Temperature Microstructure Following the Intercritical Deformation of Steel S460[J]. Journal of Iron and Steel Research, International, 2011, 18(S1):500-505.

[22] Shichen Sun, Hongze Fang, Yili Li, et al. Normalized characterization of the causes of discontinuous yield and crystal orientation deflection mechanism of β-Ti alloy during high-temperature deformation[J]. Materials Science & Engineering, A. Structural Materials: Properties, Microstructure and Processing, 2024(Feb.):893.

[23] Wei Zhou, Peng Ge, Yongqing Zhao, et al. Discontinuous Yielding in High Temperature Deformation of Ti-5553 Alloy[J]. Rare Metal Materials & Engineering, 2015, 44(10):2415-2418.

[24] Wenchen Xu, Debin Shan, Hao Zhang. Discontinuous yielding behavior of β phase containing TiAl alloy during high-temperature deformation process[J]. Acta Metallurgica Sinica - Chinese Edition-, 2013, 49(11):1339.

[25] Hao Du, Yu Gong, Binggang Liu, et al. Discontinuous Yielding Mechanisms in Tempered Hierarchical Duplex Phase Steel with High-Density Dislocations[J]. Metallurgical and Materials Transactions, A. Physical Metallurgy and Materials Science, 2022(7):53A.

[26] ISO 18265: 2013, Metallic Materials-Conversion of hardness values. International Standards Organization, 2013.

[27] Ullah S H, Ravi K. Influence of Stress Concentration and Cooling Methods on Post-Fire Mechanical Behavior of ASTM A36 Steels[J]. Construction and Building Materials, 2018, 186:920-945.

[28] Jie Lu, Hongbo Liu, Zhihua Chen, et al. Experimental investigation into the post-fire mechanical properties of hot-rolled and cold-formed steels[J]. Journal of Constructional Steel Research, 2016, 121:291-310.

[29] Weiyong Wang, Tianzi Liu. Study on Mechanical Properties of High Strength Q460 Steel after Cooling from High Temperature[J]. Journal of Building Materials, 2016.

[30] Linxin Song, Guoqiang Li. Experimental Study on Post-fire Mechanical Properties of TMCP Q550 steel[J]. Journal of Disaster Prevention and Mitigation Engineering, 2021.

[31] Guoqiang Li, Huibao Lu. Experimental research on post-fire mechanical properties of Q690 stee [J]. Journal of Building Structures, 2017, 38(05):109-116.

[32] Xiang Zeng , Wanbo Wu, Jingsi Huo, et al. Residual mechanical properties of Q890 high-strength structural steel after exposure to fire[J]. Construction and Building Materials, 2021, 304: 124661.

[33] Weiyong Wang, Yanhong Zhang, Xiang Li. Experimental study on mechanical properties of high strength Q960 steel after high temperature[J]. Journal of Building Materials, 2022, 25(01): 102-110.

[34] Xuhong Qiang, Frans S.K. Bijlaard, Henk Kolstein. Post-fire mechanical properties of high strength structural steels S460 and S690[J]. Engineering Structures, 2012, 35: 1-10.

[35] Ullah S H, Ravi K. Post-fire Mechanical Behavior of ASTM A572 Steels Subjected to High Stress Triaxialities[J]. Engineering Structures, 2019, 191(JUL.15):323-342.

[36] Lee J, Engelhardt M D, Taleff E M. Mechanical properties of ASTM A992 steel after fire[J]. Engineering Journal, 2012, 49(1): 33-44.

[37] Kai Ma, Gengwei Yang, Zhixiang Fu, et al. Effect of rolling and cooling processes on microstructure and properties of directly quenched NM400 steel [J]. Journal of Iron and Steel Research, 2025,37(01):77-85.

[38] Illarionov A G, Demakov S L, Illarionova S M, et al. Influence of Quenching Temperature on the Structure, Phase Composition, Physical and Mechanical Properties of a High-Strength Titanium Alloy of the Martensitic Class[J]. Metal Science and Heat Treatment, 2024, 66(5): 286-293.

[39] MCC Architectural Research Institute Co., Ltd. Standard for building structural assessment after fire: CECS 252:2019[M]. China Planning Press,2019.

[40] GB/T 19879-2023, Steel plate for building structure, China Standard Press, Beijing, China, 2023.